

Itinerant electron metamagnetism for lattices with van Hove density-of-states singularities near the Fermi level

F. A. Vasilevskiy,¹ P. A. Igoshev,^{1,2} and V. Yu. Irkhin^{1,2}

¹*M. N. Mikheev Institute of Metal Physics, 620108, Yekaterinburg, Kovalevskaya street, 18*

²*Ural Federal University, 620002, Russia, Yekaterinburg, Mira street, 19*

Itinerant-electron metamagnetism is investigated within the Hubbard model for various lattices having van Hove singularities (vHS) in the electronic spectrum: face-centered cubic and orthorhombic lattices. The remarkable itinerant-electron metamagnetic transition occurs provided that the Fermi level is in the region with a strong positive curvature of the density of electron states typically positioned between two close van Hove singularities. Orthorhombic distortion of tetragonal lattice is a promising mechanism for generating two closely split vHS with strong density-of-states curvature between them. A phase diagram in terms of electron filling and Hubbard interaction parameter is presented, which shows the paramagnetic-metamagnetic-ferromagnetic phase transition and regions of saturated and non-saturated magnetism. The standard Landau theory expansion based on electron density of states in the vicinity of the Fermi level is demonstrated to be insufficient to describe the whole magnetic phase diagram including the itinerant-electron metamagnetic transition.

I. INTRODUCTION

The study of magnetic phase transitions is important for a fundamental understanding of the nature of magnetism. One of the phase transition kinds is the phenomenon of itinerant-electron metamagnetism (IEMM), which is a transition from a low-magnetization state to high-magnetization state under application of a magnetic field. Although itinerant metamagnetism has been discovered for a long time, [1], a complete comprehension of this phenomenon has not yet been achieved.

Experimentally, the IEMM transition was for the first time detected in a pyrite-structure compound CoS_2 [2–4]. CoS_2 is an itinerant ferromagnet with the Curie temperature $T_c = 122$ K. There are two possible ways towards appearance of IEMM transition in this compound. The first one is the substitution of S by Se: due to broadening of the $3d$ -band with increasing Se concentration, the density of states (DOS) at the Fermi level decreases and the magnetic ordering changes. At doping values of $0.12 \leq x \leq 0.4$, $\text{Co}(\text{S}_{1-x}\text{Se}_x)_2$ becomes an exchange-enhanced Pauli paramagnet where IEMM transition in high magnetic fields $B_c < 20$ T is possible, with the critical magnetic field being smaller for smaller x [2, 4] and B_c being proportional to T^2 . The temperature dependence of magnetic susceptibility typical for metamagnetic materials is observed — a very high value of susceptibility at low temperatures as compared to Pauli paramagnets and a broad maximum at a certain temperature T_{\max} (for $\text{Co}(\text{S}_{1-x}\text{Se}_x)_2$, this is 80 K). Using the spin fluctuation theory, it has been shown that at T_{\max} there is a sign change of the fourth-order coefficient in the Landau expansion [5]; thereby T_{\max} corresponds to the temperature at which metamagnetism vanishes. The second way is also related to the broadening of the $3d$ -band due to the application of external pressure [3, 4]. With an increasing pressure, the Curie temperature for CoS_2 decreases and the ferromagnetic (FM)—paramagnetic phase transition changes its order from the second to the first one

at $p \approx 0.4$ GPa. At pressure $p > 0.4$ GPa, a metamagnetic transition above T_c is observed. The replacement S by Se results in decreasing critical pressure of this phase transition.

The next class of relevant compounds is presented by intermetallic compounds $R\text{Co}_2$ with rare earth $R=\text{Lu}$, Y. YCo_2 and LuCo_2 are typical exchange-enhanced Pauli paramagnets. The IEMM transition in them was first predicted theoretically on the basis of density functional calculations for the YCo_2 compound, the critical magnetic field value $H_c = 900$ kOe [6] being obtained, i.e., the transition occurs in strong magnetic fields. This was confirmed experimentally: the itinerant metamagnetism of compounds YCo_2 and LuCo_2 was found in strong magnetic fields $H_c = 690$ and 740 kOe, respectively [7–9]. In these compounds, an appearance of the IEMM transition is due to the hybridization of the low-energy $3d$ -band of cobalt with a high DOS and high-energy $4d(5d)$ -band of R with a relatively low DOS, resulting in a region with positive DOS curvature at the Fermi level for resulting spectrum.

The replacement of cobalt by aluminum in these compounds results in decreasing the critical magnetic field value [9–13]. This is due to the fact that such a substitution results in decreasing $3d$ -electron filling, which in turn shifts the Fermi level with the corresponding increase of DOS. Also, such a replacement leads to an increase in the volume of unit cell due to that the bandwidth narrows and DOS at the Fermi level increases. In the compound $\text{Y}(\text{Co}_{1-x}\text{Al}_x)_2$, IEMM transition is observed at $x < 0.12$, whereas at $0.12 < x < 0.20$ weak ferromagnetism occurs [14]. The temperature dependence of magnetic susceptibility has a broad maximum at T_{\max} , typical for itinerant metamagnets. Applying pressure results in an increase of H_c due to a bandwidth increase [9].

A van Hove singularity in $3d$ electron band is a possible origin of the low-spin — high spin ferromagnetic state transition in the compound LuCo_3 [15, 16].

A simple model of electron spectrum within nearest

and next-nearest neighbor hopping approximation allows to describe the magnetic properties and itinerant metamagnetic transition for double- ($n = 2$) $\text{Sr}_3\text{Ru}_2\text{O}_7$ [17] and triple-layer ($n = 3$)[18] $\text{Sr}_4\text{Ru}_3\text{O}_{10}$ ruthenates. These results suggest that an IEMM transition may have a single sufficient reason — strong positive curvature of DOS in the paramagnetic phase produced by vHS in the vicinity of Fermi level.

A typical $5f$ itinerant metamagnet is UCoAl. In magnetic fields of about 0.6 T directed along the c axis, this compound undergoes a metamagnetic transition [19, 20]. A growth of critical magnetic field with increasing pressure and temperature dependence of the susceptibility, typical for itinerant metamagnets, are observed. For $\text{UCo}_{0.98}\text{Fe}_{0.02}\text{Al}$, ferromagnetism disappears at a pressure of 0.4 GPa manifesting an IEMM transition: further pressure increasing results in linear increase of the critical magnetic field and gradual decrease of magnetization jump Δm . IEMM transition appears with increasing temperature, that is, there is a temperature-induced phase transition from the ferromagnetic state to the magnetic field-induced ferromagnetic state, predicted theoretically [21] and observed for $3d$ -band magnets [4]. The critical magnetic field grows almost linearly in T^2 at any pressure.

URhGe and UCoGe exhibit ferromagnetic and superconducting phase transitions at ambient pressure [22–24]. Features of FM transitions in these compounds are strongly dependent on the magnetic field H direction relative to the easy magnetization axis. In URhGe, in the case $H \parallel b$ at $H = H_R = 120$ kOe (the spin reorientation field) the easy magnetization axis switches from the c -axis to b -axis, and a metamagnetic transition appears. Nuclear magnetic resonance spectra show the presence of phase separation in the magnetic field $H = H_R$. The quantum critical end point of ferromagnetic (FM) wing structure appears due to the magnetic-field direction tilting from b to c axis around the H_R and is associated with field-reentrant superconductivity. Thermoelectric power measurements indicate that a Lifshitz transition occurs in a narrow window through H_R . The compound UIr_2Si_2 , being ordered antiferromagnetically at temperature below 5.5 K, exhibits metamagnetic transition occurring at 1.8 K in a magnetic field of 15.2 kOe. Despite the fact that this transition has a spin-flop character, this compound possesses some itinerant properties [25], which makes it close to itinerant metamagnets.

Density functional theory (DFT) calculations suggests that there is a set of rather weak vHS of density of states of UPt_3 in the vicinity of Fermi level. These features invoke both Lifshitz transition and non-linear dependence of magnetization on magnetic field, which is similar to an itinerant metamagnetic transition at magnetic field 20 T [26].

In the ferromagnetic $\text{La}(\text{Fe}_x\text{Si}_{1-x})_{13}$ at $x \geq 0.87$, a IEMM transition is observed at temperatures above the Curie temperature T_c [27–29]. At $x = 0.88$, the site magnetic moment arising from the metamagnetic transition

exceeds $1\mu_B$ and leads to a huge positive bulk magnetostriction of about 1.5% just above T_c [27]. The huge magnetostriction in this system is due to a huge volume change caused by the IEMM transition. The critical magnetic field at T_c is zero and increases with increasing temperature, so for $x = 0.88$ at $T_c = 195$ K the transition magnetic field near room temperature is larger than a few tens of T.

In addition, the phenomenon of itinerant metamagnetism often accompanies the giant magnetocaloric effect, e.g., in MnAs [30], $\text{Gd}_5(\text{Si}_{1-x}\text{Ge}_x)_4$ [31, 32] and $\text{MnFeP}_{1-x}\text{As}_x$ [31].

UGe_2 [22, 33, 34] and ZrZn_2 [35, 36] are itinerant ferromagnets exhibiting a first-order transition at low temperatures under pressure. T_c decreasing under pressure p and disappears at the critical pressure p_c . From thermal expansion measurements, it follows that at low pressure the transition is of a second order, but near p_c it is of a first order. Magnetic measurements for different pressures indicate first-order magnetic phase transition corresponding to a magnetization jump at a critical pressure from a low-pressure FM_2 phase with large magnetization to a high-pressure FM_1 phase with lower magnetization. Just above p_c a metamagnetic transition from the paramagnetic (PM) to the FM_1 state is observed at critical magnetic field H_c . The metamagnetic transition inside the FM phase observed in UGe_2 was explained in Ref. [37] by a double-peak structure of the electronic DOS. This particular DOS structure can also provide an explanation for the FM_1 — FM_2 transition.

Summarizing the experimental data, we can highlight the main features of itinerant metamagnets:

- 1) The magnetic susceptibility has a broad maximum near the temperature T_{max} ;
- 2) The value of the critical magnetic field H_c of a IEMM transition is proportional to T^2 at low temperatures;
- 3) IEMM transition characteristics are very sensitive to external pressure and doping.

On one hand, itinerant metamagnetic transition can occur in an electronic system where magnetism has an itinerant nature. On the other hand, for the occurrence of a metamagnetic transition, it is necessary that the electronic structure of the system has significant features of the DOS: the condition for the occurrence of metamagnetism is a positive DOS curvature ($d^2\rho/d\epsilon^2 > 0$) at the Fermi level [38, 39]. One of such mechanisms can be presence of van Hove singularities in the electronic spectrum [40]. Modern DFT calculation methods allow to calculate the density of states in the Kohn-Sham spectrum, which can be used as a starting point for further studies, including simple mean-field approaches or advanced approaches taking into account for magnetic fluctuations and correlation effects.

The papers [37, 41–43] discuss the microscopic approach to the study of IEMM. In Ref. 44 the onset of a ferromagnetic ordering in the non-degenerate Hubbard model on a face-centered cubic (FCC) lattice within

the framework of the functional renormalization group method is investigated; the hopping integral configuration was taken to provide a giant van Hove singularity in DOS. In particular, it was shown that correlation effects can be taken into account for three-dimensional lattices in the framework of the Stoner theory by renormalizing the electron-electron interaction parameter U , which takes into account its screening in the partial-particle channel. Magnetic phase separation for FM-PM phase transition was considered within the Landau theory generated by giant vHS in FCC lattice [45].

The aim of the present work is to study the metamagnetic phase transition in metals having van Hove singularities in the electronic spectrum. The following lattices are considered: (1) a square lattice with an anisotropic spectrum (rectangular lattice) in the nearest-neighbor and next-nearest-neighbor approximation, where the transfer integrals between nearest neighbors depend on the bond direction, which provides a pair of DOS peaks and a region between them with large curvature; (2) an orthorhombic lattice obtained from a rectangular lattice by adding a transfer along the z -axis, which leads to a change of the two-peak structure of DOS to two-plateau structure and preservation of the region with positive curvature $\rho(\epsilon)$; (3) FCC lattice with small τ ($\tau = t/t'$, t (t') being nearest-neighbor (next-nearest-neighbor) hopping integral); (4) FCC lattice with τ in the vicinity of $-1/2$ ($\tau = -0.52$ and -0.54) has a DOS singularity in the form of van Hove plateau, corresponding to giant vHS (at $\tau = -1/2$), and a considerable DOS curvature [40, 45, 46].

II. ELECTRON SPECTRUM AND HARTREE-FOCK APPROXIMATION EQUATIONS

The non-degenerate Hubbard model Hamiltonian reads

$$\mathcal{H} = \sum_{ij\sigma} t_{ij} a_{i\sigma}^\dagger a_{j\sigma} + U \sum_i n_{i\uparrow} n_{i\downarrow} - h \sum_{i\sigma} \sigma n_{i\sigma}, \quad (1)$$

where t_{ij} is hopping integral between sites i and j , U is a Coulomb interaction parameter, $h = \mu_B H$ is magnetic field in energy units with μ_B being the Bohr magneton, $a_{i\sigma}^\dagger, a_{i\sigma}$ are the creation and annihilation electron operators, $n_{i\sigma} = a_{i\sigma}^\dagger a_{i\sigma}$ is the electron number operator at lattice site i with z axis spin projection $\sigma = \pm 1$.

Below, we study the thermodynamics of the IEMM transition in the Hartree-Fock approximation (HFA). The free energy in this approximation has the form [47]

$$F_{\text{HF}}(T, n, h|m) = F_0(T, n|m) + (U/4)(n^2 - m^2) - hm, \quad (2)$$

where the free energy of the electron gas

$$F_0(T, n, m) = \Omega_0(T, E_F, \Delta) + m \cdot \Delta + n \cdot E_F \quad (3)$$

is defined through the Legendre transformation of the grand potential for free electron gas,

$$\Omega_0(T, E_F, \Delta) = -T \sum_{\mathbf{k}\sigma} \ln(1 + \exp(-\beta(\epsilon_{\mathbf{k}} - \sigma\Delta - E_F))), \quad (4)$$

where $\beta = 1/T$ (temperature T is taken in energy units), the Fermi level $E_F = E_F(n, m)$ and spin subband splitting $\Delta = \Delta(n, m)$ are determined from the equations

$$\frac{\partial \Omega_0}{\partial E_F} + n = 0, \quad (5)$$

$$\frac{\partial \Omega_0}{\partial \Delta} + m = 0. \quad (6)$$

We rewrite these equations as the equations

$$n = \sum_{\sigma} \int d\epsilon \rho(\epsilon) f_{\mu} \left(\epsilon + \frac{Un}{2} - \sigma\Delta \right), \quad (7)$$

$$m = \sum_{\sigma} \sigma \int d\epsilon \rho(\epsilon) f_{\mu} \left(\epsilon + \frac{Un}{2} - \sigma\Delta \right) \quad (8)$$

for the site magnetization m in units of μ_B and chemical potential μ for given values of U , filling n , and magnetic field h . Here $f_{\mu}(E) = (\exp((E - \mu)/T) + 1)^{-1}$ is the Fermi function, $\mu = E_F + Un/2$, $\Delta = Um/2 + h$, $\rho(\epsilon)$ is DOS for an electron spectrum $\epsilon_{\mathbf{k}} = (1/N) \sum_{ij} t_{ij} \exp[i\mathbf{k}(\mathbf{R}_i - \mathbf{R}_j)]$

$$\rho(\epsilon) = \frac{1}{N} \sum_{\mathbf{k}} \delta(\epsilon - \epsilon_{\mathbf{k}}), \quad (9)$$

where $w_1 < \epsilon < w_2$, $w_{1,2}$ being band boundaries. Main equations (7),(8) have, generally speaking, several solutions

$$m = m_i(T, n, h), \quad (10)$$

indexed by i . If more than one solution is obtained, the solution with the lowest free energy (2) is chosen. The IEMM transition point corresponds to the fact that two different solutions Eq. (10) have equal free energy at some magnetic field $h > 0$:

$$F_{\text{HF}}(T, n, h|m_1) = F_{\text{HF}}(T, n, h|m_2). \quad (11)$$

The equation (11) can be viewed as an equation on the critical magnetic field $h = h_c(T, n)$. A saturated FM state is realized when effective Fermi level of lower spin subband $E_F - (Um/2 + h)$ is positioned below w_1 .

Note that the well-known Stoner criterion

$$U\rho(E_F) > 1 \quad (12)$$

corresponds to the condition of existence of the local maximum of the ground-state free energy $F_{\text{HF}}(T, n, h = 0|m)$ at $m = 0$ in zero magnetic field, see Eq. (2). Thus, the fulfillment of the Stoner criterion has an exact meaning of the impossibility of a paramagnetic (PM) state even as a metastable one.

The spectrum of *rectangular* (anisotropic square) lattice in the nearest- and next-nearest-neighbor approximation has the form

$$\epsilon_{\mathbf{k}}^{\text{R}}(\tau_a, \tau) = -2t[\cos k_x + \tau_a \cos k_y + 2\tau \cos k_x \cos k_y], \quad (13)$$

where $\tau_a = t_{\perp}/t$, $\tau = t'/t$, t is the hopping integral along x , t_{\perp} along y , t' along the diagonal. Without loss of generality, we assume $\tau_a < 1$. Here and below lattice parameter is taken as unity.

The spectrum (13) produces DOS of rectangular lattice with bandwidth $W_{\text{R}} = (\max[w_1, E_2] - E_{\text{min}})$ by a direct calculation:

- $\tau < \tau_a/2$:

$$\rho_{\text{R}}(\epsilon, \tau_a, \tau) = \frac{1}{\pi^2 t} \frac{1}{\sqrt{|(1 - \tau_a)^2 - (\epsilon/(2t) - 2\tau)^2|}} \times \begin{cases} \mathbb{K} \left(\frac{(1 + \tau_a)^2 - (\epsilon/(2t) + 2\tau)^2}{(1 - \tau_a)^2 - (\epsilon/(2t) - 2\tau)^2} \right), & E_{\text{min}} < \epsilon < E_1, \\ \mathbb{K} \left(1 - \frac{(1 + \tau_a)^2 - (\epsilon/(2t) + 2\tau)^2}{(1 - \tau_a)^2 - (\epsilon/(2t) - 2\tau)^2} \right), & E_1 < \epsilon < E_2, \\ \mathbb{K} \left(\frac{(1 + \tau_a)^2 - (\epsilon/(2t) + 2\tau)^2}{(1 - \tau_a)^2 - (\epsilon/(2t) - 2\tau)^2} \right), & E_2 < \epsilon < w_1; \end{cases} \quad (14)$$

- $\tau_a/2 < \tau < 1/2$:

$$\rho_{\text{R}}(\epsilon, \tau_a, \tau) = \frac{1}{\pi^2 t} \frac{1}{\sqrt{|(1 - \tau_a)^2 - (\epsilon/(2t) - 2\tau)^2|}} \times \begin{cases} \mathbb{K} \left(\frac{(1 + \tau_a)^2 - (\epsilon/(2t) + 2\tau)^2}{(1 - \tau_a)^2 - (\epsilon/(2t) - 2\tau)^2} \right), & E_{\text{min}} < \epsilon < E_1, \\ \mathbb{K} \left(1 - \frac{(1 + \tau_a)^2 - (\epsilon/(2t) + 2\tau)^2}{(1 - \tau_a)^2 - (\epsilon/(2t) - 2\tau)^2} \right), & E_1 < \epsilon < w_1. \end{cases} \quad (15)$$

$$\rho_{\text{R}}(\epsilon, \tau_a, \tau) = \frac{1}{\pi^2 t} \frac{1}{\sqrt{|(1 + \tau_a)^2 - (\epsilon/(2t) + 2\tau)^2|}} \times \mathbb{K} \left(\frac{(1 - \tau_a)^2 - (\epsilon/(2t) - 2\tau)^2}{(1 + \tau_a)^2 - (\epsilon/(2t) + 2\tau)^2} \right), \quad w_1 < \epsilon < E_2. \quad (16)$$

- $1/2 < \tau$:

$$\rho_{\text{R}}(\epsilon, \tau_a, \tau) = \frac{1}{\pi^2 t} \begin{cases} \frac{\mathbb{K} \left(\frac{(1 + \tau_a)^2 - (\epsilon/(2t) + 2\tau)^2}{(1 - \tau_a)^2 - (\epsilon/(2t) - 2\tau)^2} \right)}{\sqrt{|(1 - \tau_a)^2 - (\epsilon/(2t) - 2\tau)^2|}}, & E_{\text{min}} < \epsilon < w_1, \\ 2 \frac{\mathbb{K} \left(\frac{(1 + \tau_a)^2 - (\epsilon/(2t) + 2\tau)^2}{(1 - \tau_a)^2 - (\epsilon/(2t) - 2\tau)^2} \right)}{\sqrt{|(1 - \tau_a)^2 - (\epsilon/(2t) - 2\tau)^2|}}, & w_1 < \epsilon < w_2, \\ 2 \frac{\mathbb{K} \left(\frac{(1 - \tau_a)^2 - (\epsilon/(2t) - 2\tau)^2}{(1 + \tau_a)^2 - (\epsilon/(2t) + 2\tau)^2} \right)}{\sqrt{|(1 + \tau_a)^2 - (\epsilon/(2t) + 2\tau)^2|}}, & w_2 < \epsilon < E_1, \\ \frac{\mathbb{K} \left(\frac{(1 - \tau_a)^2 - (\epsilon/(2t) - 2\tau)^2}{(1 + \tau_a)^2 - (\epsilon/(2t) + 2\tau)^2} \right)}{\sqrt{|(1 + \tau_a)^2 - (\epsilon/(2t) + 2\tau)^2|}}, & E_1 < \epsilon < E_2, \end{cases} \quad (17)$$

where $\mathbb{K}(x) = \int_0^{\pi/2} (1 - x \sin^2 \phi)^{-1/2} d\phi$ is the full elliptic integral of the first kind,

$$E_{\text{min}} = 2t(-1 - \tau_a - 2\tau), \quad (18)$$

$$E_1 = 2t(-1 + \tau_a + 2\tau), \quad (19)$$

$$E_2 = 2t(1 - \tau_a + 2\tau), \quad (20)$$

$$\omega_1 = 2t(1 + \tau_a - 2\tau), \quad (21)$$

$$\omega_2 = t\tau_a/\tau. \quad (22)$$

At $\tau_a = 1$, the spectrum of the square lattice without anisotropy with one van Hove peak of the density of states is realized, see Fig. 1 [48]. As τ_a decreases, point symmetry of the lattice is broken and this peak splits into two ones. A strong curvature of DOS should be realized between the peaks. In the context of IEMM transition, it is promising to set the PM phase Fermi level between the peaks.

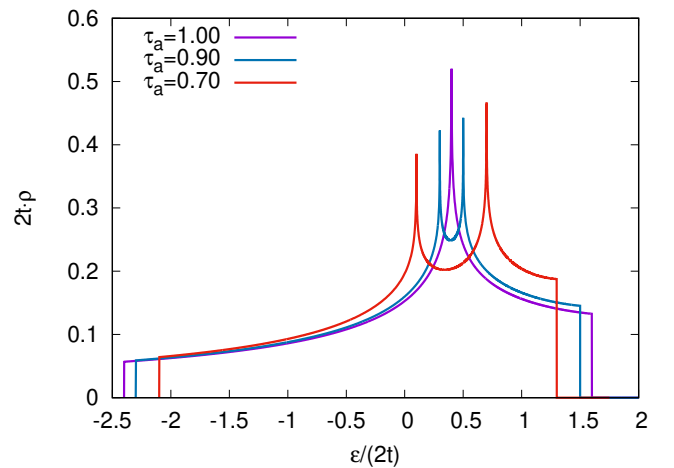


FIG. 1. Densities of states $\rho_{\text{R}}(\epsilon, \tau_a, \tau)$ of the rectangular lattice for different values of τ_a , at $\tau = 0.20$.

For $\tau < 0.5$, there are two van Hove saddle-type points in the spectrum at $\mathbf{k} = (0, \pi), (\pi, 0)$, the corresponding energy is $\epsilon = \epsilon_X = 4\tau t$. These points produce a logarithmic van Hove singularity. When anisotropy is taken into account, the energies at the saddle points cease to coincide and the van Hove peak splits into two peaks with the energies $\epsilon_{X,\pm} = 4t + 2t\tau \pm (1 - \tau_a)$. We consider two cases: 1) the strongly anisotropic case $\tau_a = 0.70$, $\tau = 0.20$; 2) the weakly anisotropic case $\tau_a = 0.90$ and $\tau = 0.20$, when τ_a is close to unity.

The spectrum of a rectangular lattice can be extended to a three-dimensional case — orthorhombic (OR) lattice including the hopping integral $t_z = t\tau_z$ along z axis bond. Then, instead of one van Hove point, there appears a plateau (cf. [49, 50]), see Fig. 2. At that, the DOS ρ_{OR} between vHS levels preserves a strong curvature in two cases: 1) very small value τ_z , we choose $\tau = 0.01$, see Fig. 2(a); 2) sufficiently large value of τ_z at small value of τ_a , we choose $\tau_a = 0.5$, $\tau_z = 0.2$, see Fig. 2(b). Increasing the hopping integral along the z axis leads to

plateau broadening and to large distortions of the rectangular lattice, so that preservation of the region with strong curvature is possible with increasing the energy distance between vHS positions (decreasing τ_a).

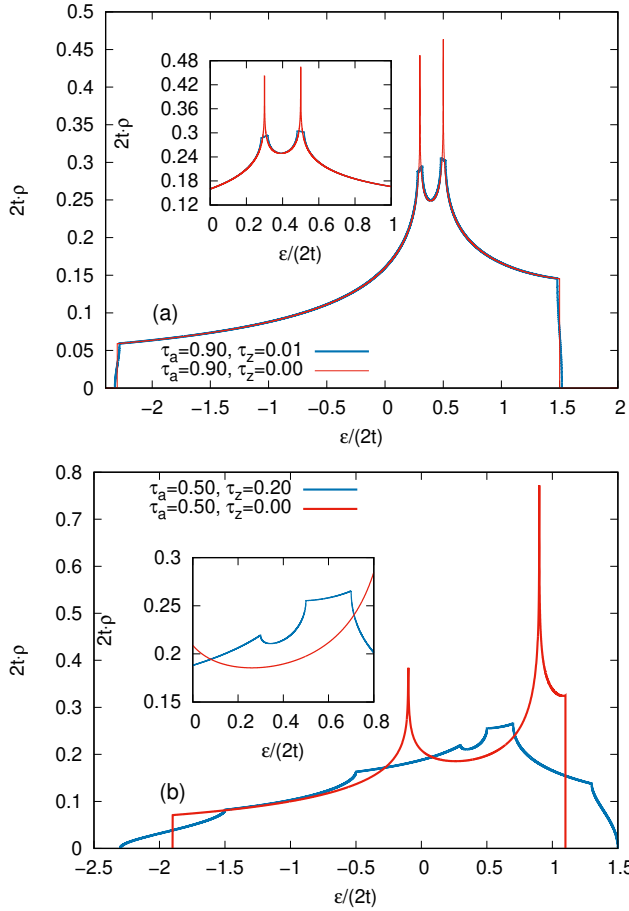


FIG. 2. Density of states $\rho_{\text{OR}}(\epsilon, \tau_a, \tau, \tau_z)$ of OR ($\tau_z \neq 0$) and rectangular $\rho_{\text{R}}(\epsilon, \tau_a, \tau)$ ($\tau_z = 0$) lattice for $\tau = 0.20$. In the inset, the region of DOS near van Hove singularities is shown. (a) $\tau_a = 0.90$, $\tau_z = 0.01$; (b) $\tau_a = 0.50$, $\tau_z = 0.20$.

The electron spectrum for FCC lattice in the nearest- and next-nearest-neighbor approximation has the following form

$$\epsilon_{\mathbf{k}}^{\text{FCC}}(\tau) = \left[4 \left(\cos \frac{k_x}{2} \cos \frac{k_y}{2} + \cos \frac{k_x}{2} \cos \frac{k_z}{2} + \cos \frac{k_y}{2} \cos \frac{k_z}{2} \right) - 2\tau(\cos k_x + \cos k_y + \cos k_z) \right] t. \quad (23)$$

In the nearest-neighbor approximation, a logarithmic divergence in the dependence of $\rho_{\text{FCC}}(\epsilon, \tau)$ at $\tau = 0$ appears at the bottom of the band, see Fig. 3 [51]. Near this feature, there is a region with strong positive DOS curvature, which can lead to appearance of IEMM transition.

In the case of small hopping between the next-nearest neighbors $\tau = 0.05$, the logarithmic divergence of DOS

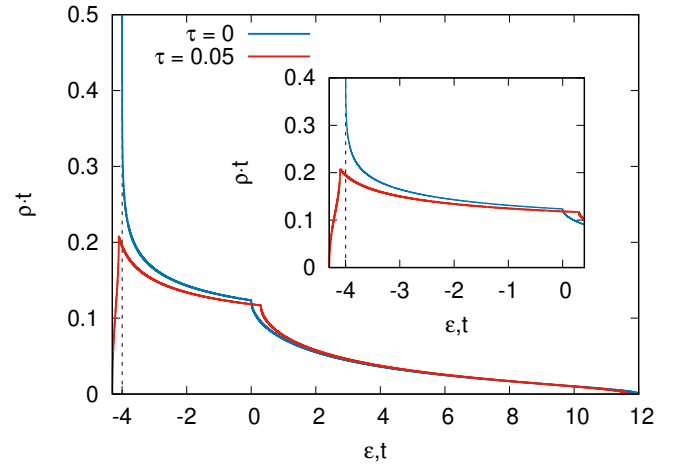


FIG. 3. The density of states $\rho_{\text{FCC}}(\epsilon, \tau)$ for the FCC lattice for $\tau = 0$ and $\tau = 0.05$. The inset shows the high-curvature region near the band bottom.

at the band bottom becomes smeared and strong DOS curvature is preserved, see Fig. 3.

At $\tau = -0.5$ we have giant (higher-order, quasi-one-dimension) vHS at the band bottom for FCC lattice with strong curvature [52]. Such a case is ideal and probably not realizable, so that we consider cases of τ which are close to -0.5 . In the spectrum, the ratios of the transfer integral between the sites $\tau = -0.52$ and -0.54 are taken into account, which ensures the appearance of a DOS feature in the form of a van Hove plateau and a region with a strong DOS curvature, see Fig. 4 and Ref. [40]. Consideration of several values of τ will allow us to understand the impact of the DOS curvature on the IEMM phenomenon.

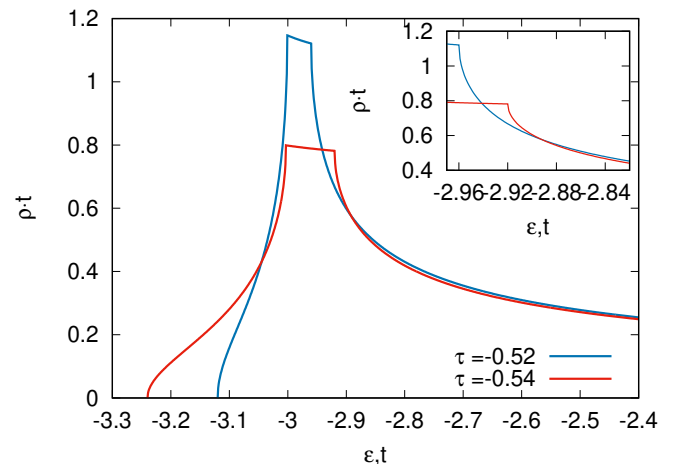


FIG. 4. The density of states $\rho_{\text{FCC}}(\epsilon, \tau)$ for the FCC lattice for $\tau = -0.52$ and $\tau = -0.54$. The inset shows the region of DOS where IEMM transition is considered, see below.

III. RESULTS

In this Section, the itinerant metamagnetic transition is investigated for the above-mentioned DOS's using numerical solution of Eqs. (7–8). Eq. (2) is used to determine the solution $m = m_i(T, n, h)$ with minimal free energy $F(T, n, h|m)$ for particular T and h .

A. Rectangular lattice

In this subsection we consider the IEMM transition for a rectangular lattice, see Sect. II.

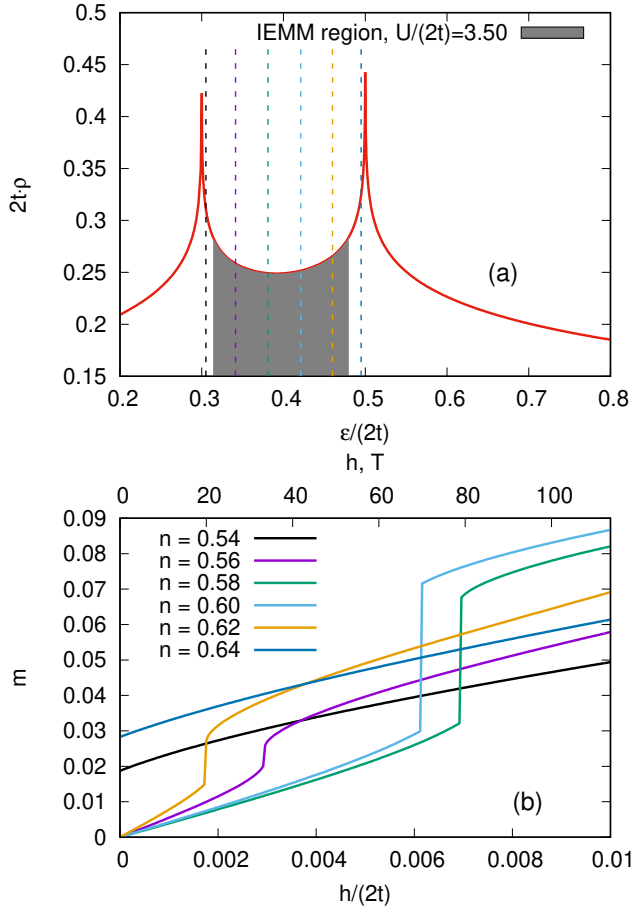


FIG. 5. (a) Density of states of a rectangular lattice $\rho_R(\epsilon, \tau_a, \tau)$ at $\tau = 0.20$. The vertical lines indicate PM phase Fermi level E_F corresponding to the chosen filling n . Filling shows the region in which the IEMM transition occurs at a given $U = 7.00t$. (b) Magnetic field dependence of magnetization $m(h)$ for rectangular lattice $\tau_a = 0.90$, $\tau = 0.20$ at $T = 0.004t$, $U = 7.00t$. The upper axis shows h_c in units of T , see text.

Choosing the filling where the Fermi level falls in the region between a pair of vHS levels, see Fig. 5(a), we first study the magnetic field dependence $m = m_i(T, n, h)$ for the case of a weak anisotropy, $\tau_a = 0.90$, $\tau = 0.20$ (see Fig. 5(b)), at low temperature $T = 4 \cdot 10^{-3}t$ and $U = 7t$.

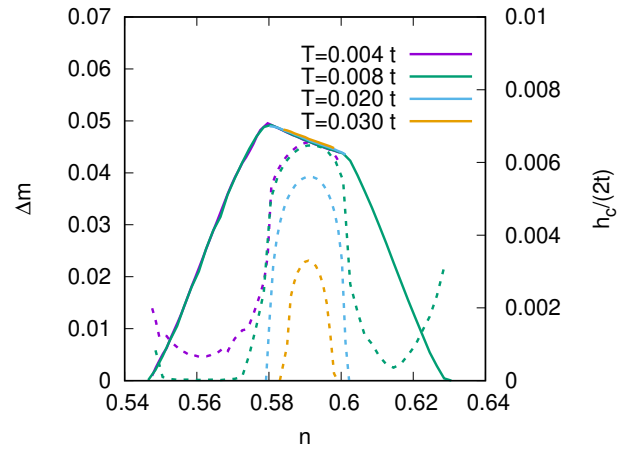


FIG. 6. Dependences of magnetization jump Δm (dashed line, left axis) and critical magnetic field h_c (solid line, right axis) on filling for rectangular lattice $\tau_a = 0.90$, $\tau = 0.20$ at different temperatures at $U = 7.00t$.

This dependence is typical for IEMM transition: at certain value of the external magnetic field, the magnetization exhibits a magnetization jump Δm indicating a first-order IEMM phase transition. For convenience of comparison with typical experimental values, we choose the reference value of the bandwidth $W = W_R = 7.6t$ to be 5 eV bandwidth.

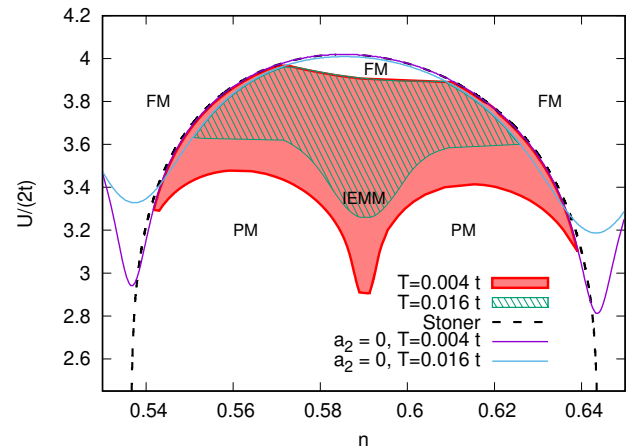


FIG. 7. Phase diagram in $U - n$ plane for the rectangular lattice $\tau_a = 0.90$, $\tau = 0.20$ at $T = 0.004t$ and $0.016t$ with ferromagnetic (FM) and paramagnetic (PM) phases, and region of IEMM transition. The dashed line indicates the curve corresponding to the Stoner criterion $U\rho(E_F) = 1$. Solid blue at $T = 0.016t$ and magenta at $T = 0.004t$ lines corresponds to $a_2 = 0$, see below section IV.

Important IEMM characteristics are the magnetization jump Δm and the critical magnetic field h_c — the magnetic field value at which Δm occurs. The filling dependence of these characteristics at different temperatures are shown in Fig. 6. Whereas the dependence $\Delta m(n)$ is strongly non-monotonous, the $h_c(n)$ depen-

dence is dome-like and exhibits two kinks. Thus, at $U = 7t$ the IEMM transition region ($0.55 \lesssim n \lesssim 0.63$) is inside the FM phase region. When a PM phase Fermi energy approaches the minimum of $\rho(E_F)$, the Δm and h_c are close to their maximum. With increasing temperature, the transition region narrows, the maximum value of the magnetization jump decreases, while the critical field filling dependence remains almost unchanged.

To characterize the U dependence of IEMM transition, a phase diagram is calculated in the variables $U - n$ (see Fig. 7) at two temperature values $T = 4 \times 10^{-3}$ and $1.6 \times 10^{-2}t$. The region bounded by red curves corresponds to IEMM region; the dashed line indicates the curve corresponding to the parameters U and n , for which the Stoner criterion is fulfilled.

At the lower boundary of IEMM region, transition is not observed in the whole filling interval between the curves of fulfillment of the Stoner criterion, and regions corresponding to PM phase appear. In this case, IEMM transition occurs near the edge and the center of this filling interval. The latter is connected to the region with maximal DOS curvature.

At the U values from $7.00t$ to $7.60t$, the filling interval of IEMM region is of maximum length. In this case, the IEMM transition is observed for any position of PM phase Fermi level between the peaks. Moving away from IEMM region in filling forces first-order phase transition to FM phase.

At larger values of U (upper part of the diagram), the IEMM transition region is not bounded by the dashed line corresponding to the Stoner criterion. In the region between IEMM and FM phase regions, there is a FM region, in contrast to the Stoner criterion.

The temperature increase gradually suppresses the IEMM transition region at lower U -boundary (see Fig. 7). At the upper U -boundary, the IEMM transition is almost not affected by the temperature increase. The $a_0 = 0$ curves are strongly affected as temperature increases only at the edges of Stoner criterion's dome.

For the case of strongly anisotropic spectrum $\tau_a = 0.70$, $\tau = 0.20$ at $T = 0.004t$, $U = 8.20t$ the magnetic field dependence $m(T, n, h)$ has a form, similar to the case of weakly anisotropic spectrum (see Fig. 8), but the IEMM transition occurs at larger h_c and Δm reaches larger values. Then the filling interval corresponding to the IEMM transition increases. This is due to an increase in the energy difference between vHS's positions of ρ_R and corresponds to an increase of the region with strong DOS curvature.

B. Orthorhombic lattice

A more realistic case is the spectrum including the hopping along the z -axis, so that the rectangular lattice transforms into orthorhombic one. For instance, we consider two cases in which the region with strong curvature of the density of states is preserved at $\tau = 0.2$: small

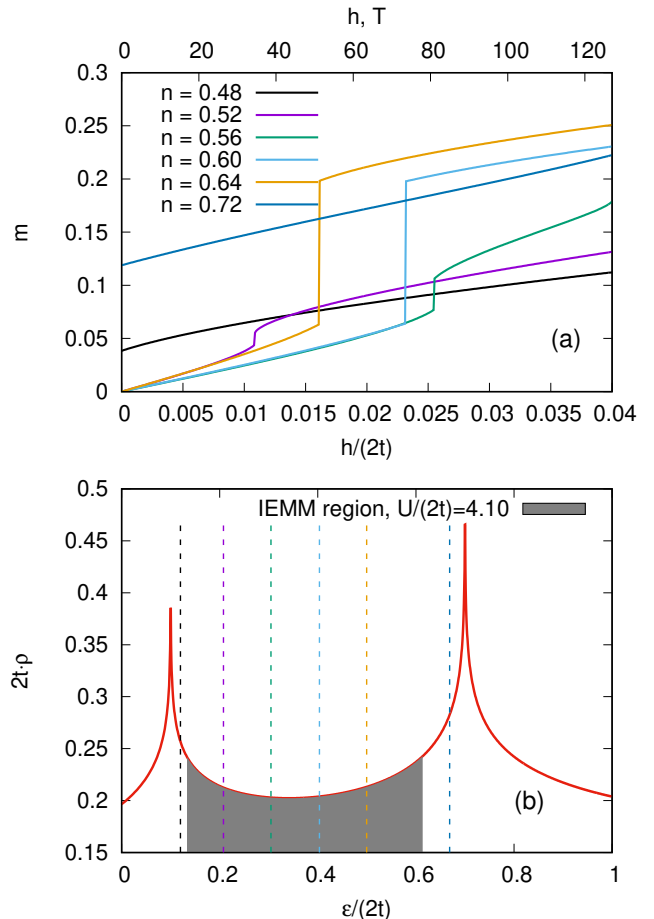


FIG. 8. (a) The same as for Fig. 5 (b) for rectangular lattice $\tau_a = 0.70$, $\tau = 0.20$ at $T = 0.004t$, $U = 8.20t$. (b) The same as for Fig. 5 (a) for rectangular lattice $\rho_R(\epsilon, \tau_a, \tau)$ at $\tau = 0.20$.

$\tau_z = 0.01$ and $\tau_a = 0.90$ (see Fig. 2 (a)); large $\tau_z = 0.20$ and $\tau_a = 0.50$ (see Fig. 2 (b)).

In the case of the OR lattice with $\tau_z = 0.01$, $\tau_a = 0.90$, $\tau = 0.20$, for the same parameters as considered above for the rectangular lattice ($U = 7.00t$, $T = 0.004t$), magnetic field dependence of the magnetization is shown, see Fig. 9(a). One can see that the IEMM transition for the OR lattice is partially suppressed at the edge of the IEMM filling interval for the rectangular lattice. The comparison of the $U - n$ phase diagrams for rectangular and OR lattices is presented in Fig. 10. The replacement of DOS peaks by plateaus results in a decrease in the IEMM region, so that the transition is possible only at $U > 6.6t$.

We consider the case $\tau_z = 0.20$, $\tau_a = 0.50$. Increasing the hopping along the z -axis causes the size of both plateaus to increase and the region with positive DOS curvature to decrease. At a certain value of τ_z , the plateaus merge and the region with strong DOS curvature disappears. To preserve this region at larger values of τ_z , it is necessary to increase the distance between the two plateaus. For this purpose we reduced the parameter τ_a , see Fig. 9(b).

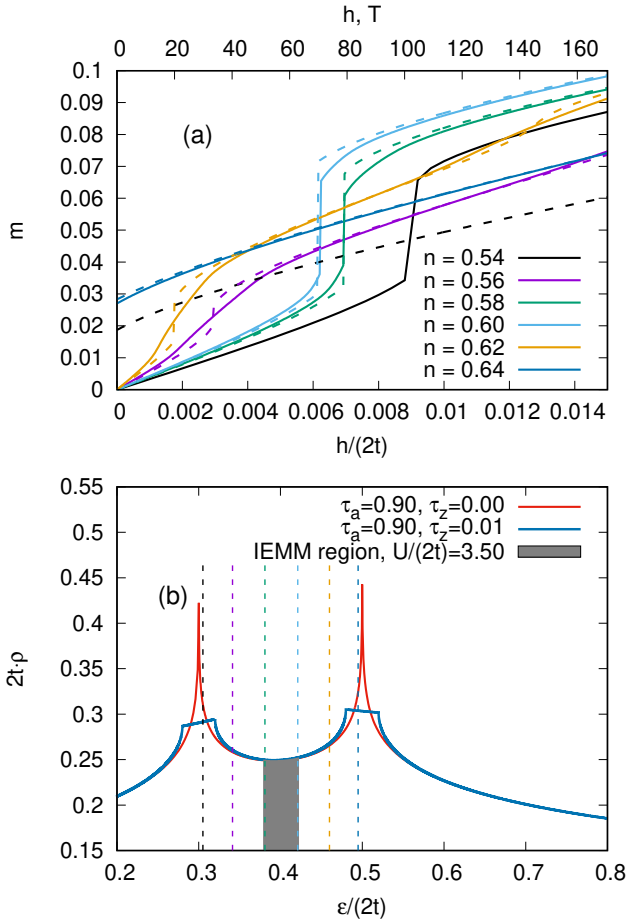


FIG. 9. The same as for Fig. 5 (b) for OR lattice $\tau_z = 0.01$ (solid line) and the rectangular lattice (dashed line) $\tau_a = 0.90$, $\tau = 0.20$ at $T = 0.004t$, $U = 7.00t$. (b) The same as for Fig. 5 (a) for a rectangular and a OR lattice.

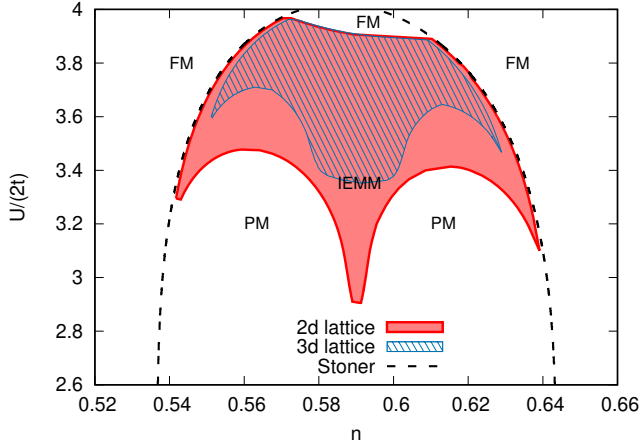


FIG. 10. Phase diagram in $U - n$ variables at $T = 0.004t$ for rectangular and OR lattice $\tau_z = 0.01$, $\tau_a = 0.90$, $\tau = 0.20$. The dashed line indicates the curve corresponding to the Stoner criterion $U\rho(E_F) = 1$.

In this case, the magnetic field dependence of magneti-

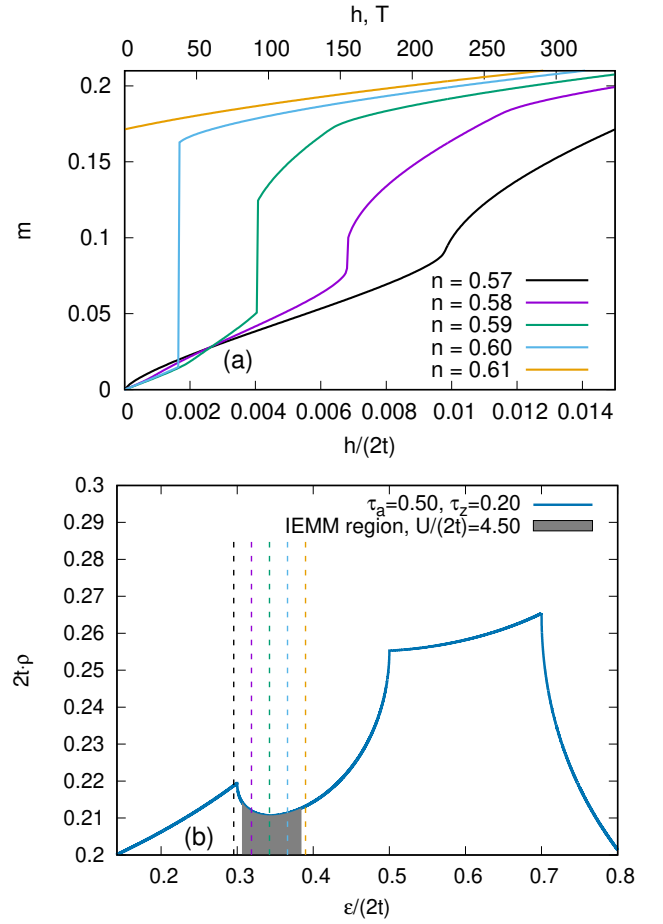


FIG. 11. The same as for Fig. 5 (b) for OR lattice $\tau_z = 0.20$, $\tau_a = 0.50$, $\tau = 0.20$ at $T = 0.004t$, $U = 9.00t$. (b) The same as for Fig. 5 (b) for OR lattice $\rho_R(\epsilon, \tau_a, \tau, \tau_z)$ at $\tau = 0.20$.

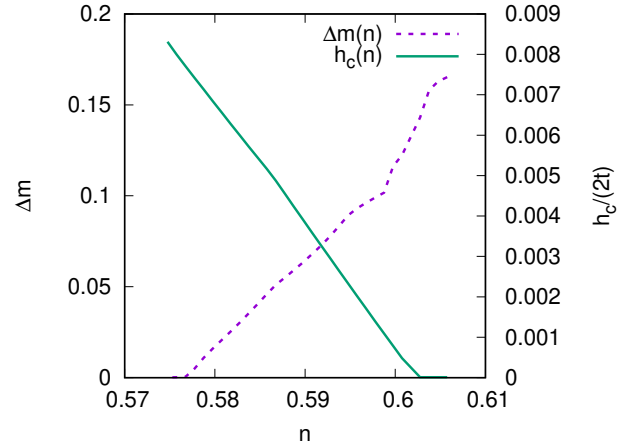


FIG. 12. The same as for Fig. 6 for OR lattice $\tau_z = 0.20$, $\tau_a = 0.50$, $\tau = 0.20$ at $T = 0.004t$, $U = 9.00t$.

zation for $U = 9.00t$ is presented in Fig. 11(a). The PM phase Fermi energy at the chosen filling values is in the region with positive curvature near the left plateau, see Fig. 11(b). The increase of filling results in monotonous

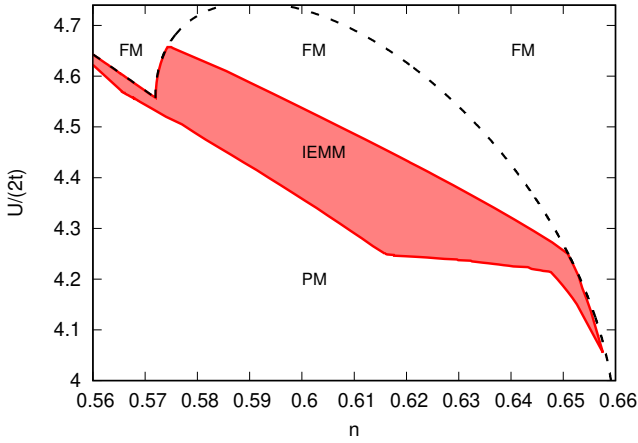


FIG. 13. Phase diagram in $U - n$ variables at $T = 0.004t$ for OR lattice $\tau_z = 0.20$, $\tau_a = 0.50$, $\tau = 0.20$. The dashed line indicates the curve corresponding to the Stoner criterion $U\rho(E_F) = 1$. The strong difference of FM condition from the Stoner one originates from the first order transition, see below in the section IV.

increasing the magnetization jump Δm and decreasing the critical field h_c (see Fig. 12).

For this case, the phase diagram in $U - n$ variables is shown in Fig. 13. The kink of IEMM transition line at $n = 0.575$ is caused by crossing of the PM Fermi level and the vHS energy level, see Fig 11(b). This situation substantially differs from that considered above for a rectangular lattice (cf. Fig. 7). Decreasing the parameter U leads to a shift of the IEMM transition region towards larger n , which does not agree with the Stoner criterion curve behavior.

C. FCC lattice

In this Section we treat IEMM transition in the 3D FCC lattice for the cases of small τ and $\tau \simeq -0.5$. Both these cases correspond to strong vHS. We choose the reference value of the bandwidth $W = 16t$ for $\tau = 0$, $\tau = 0.05$ and $W = 18t$ for $\tau \simeq -0.5$ to be 5 eV .

1. $\tau = 0$

The dependence of the density of states for the FCC lattice spectrum in the nearest-neighbor hopping approximation ($\tau = 0$) has a logarithmic divergence at the band bottom, see Fig. 3(a) in Sec. II. As a consequence, a region with positive curvature $\rho(\epsilon)$ appears at the bottom of the band, which, as in the case of an orthorhombic lattice, can lead to IEMM transition when PM phase Fermi level is positioned in high-curvature region between two vHS levels.

The magnetic field magnetization dependence for this case is shown in Fig. 14(a) and the positions of PM phase

Fermi level on DOS plot corresponding to different filling values are shown in Fig. 14(b). One can see that the IEMM transition to saturated FM is observed. A filling increase leads to a monotonous decrease in Δm and an increase in h_c (see Fig. 15). While DOS plot seems to be different from that for the rectangular lattice, some similarity (large critical magnetic field values) of these two cases is due to the fact that there is strong curvature region between two vHS peculiarities of DOS in both the cases.

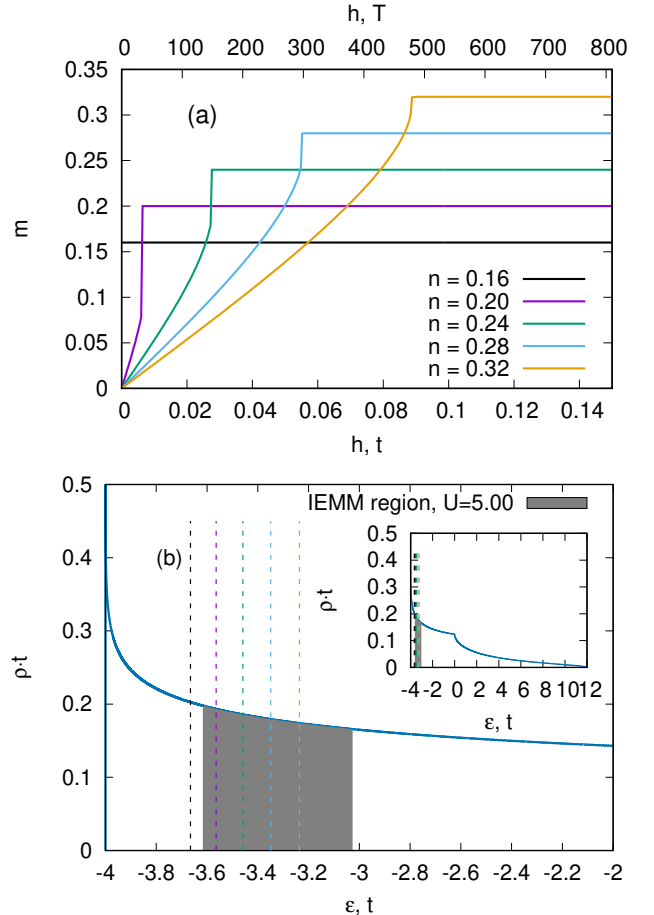


FIG. 14. (a) The same as for Fig. 5(b) for FCC lattice $\tau = 0$, at $T = 0.002t$, $U = 5.00t$. (b) The same as for Fig. 5 (a) for FCC lattice $\rho_{\text{FCC}}(\epsilon, \tau = 0)$.

The $U - n$ phase diagram at $T = 0.002t$ is presented in Fig. 16. In this case, the broad IEMM region located between the two vHS levels separates two phases: PM from below and FM from above. The saturation boundary, being in the region of IEMM transition, separates the regions of saturated and unsaturated magnetism in critical fields. Almost in all regions of metamagnetic transition, there is saturated magnetism in h_c , only at $U > 6.80t$ the saturation boundary goes to the FM region. In the FM region, the saturation boundary already separates saturated and unsaturated ferromagnetism.

There are large Δm and h_c values in this case, which is related to large energy interval of high DOS curvature.

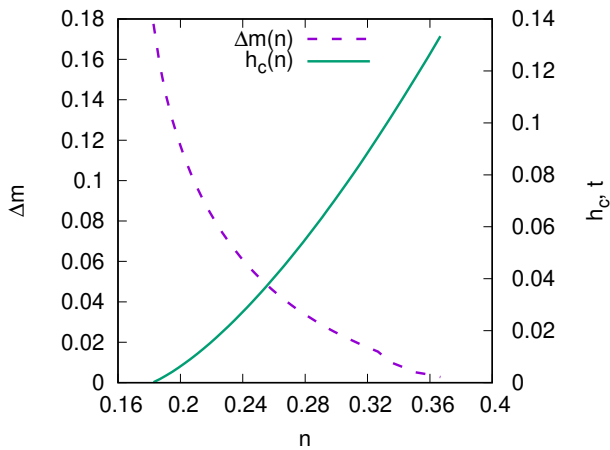


FIG. 15. The same as for Fig. 6 for FCC lattice at $\tau = 0$, $T = 0.002t$, $U = 5.00t$.

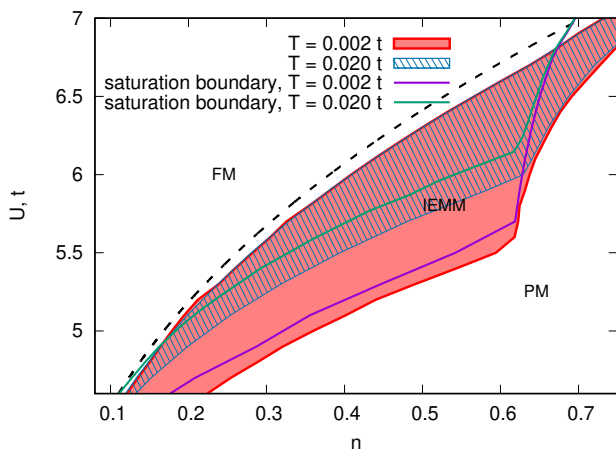


FIG. 16. Phase diagram in $U - n$ variables for FCC lattice for $\tau = 0$ at different temperatures: FM is ferromagnetic region, PM is paramagnetic region. Within the latter, filled IEMM areas correspond to metamagnetism regions. The dotted line indicates the curve corresponding to the Stoner criterion $U\rho(E_F) = 1$, the saturation boundary line divides the region of saturated and unsaturated magnetism at $T = 0.002t$ and $0.020t$.

The same anomalously large critical magnetic fields of IEMM transition, and even larger ones are observed for a square lattice with $\tau = 0.35$ [43], where IEMM transition is also caused by the strong curvature of DOS between the vHS peak and the vHS at the bottom or top of the band.

2. $\tau = 0.05$

A more realistic case of the spectrum for the FCC lattice is that taking into account the next-nearest hopping integral. We assume it to be small, $\tau = 0.05$. Then the divergence at the bottom of the band observed at $\tau = 0$

is replaced by a plateau in the vicinity of band bottom, see Fig. 17(a).

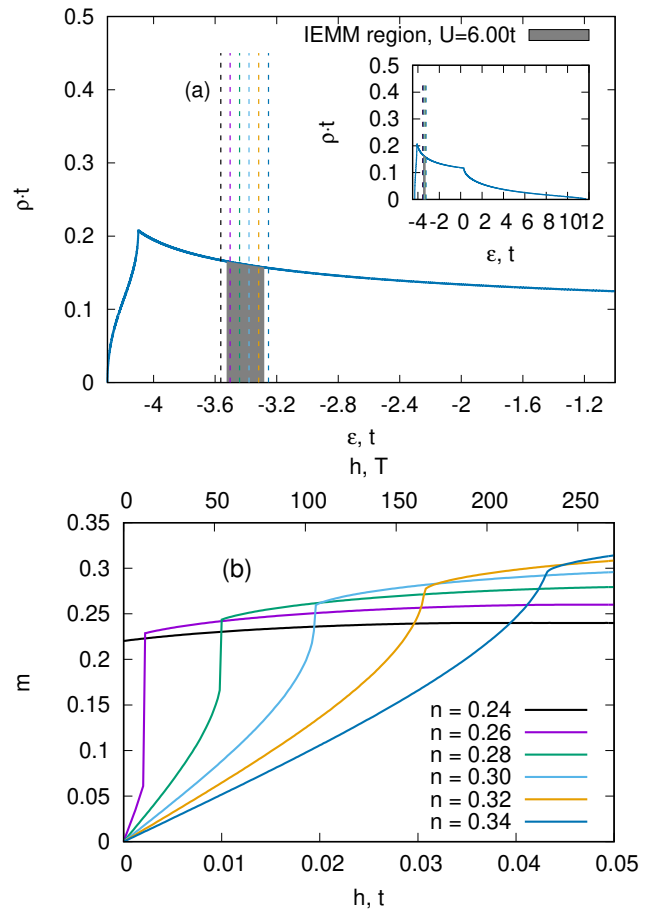


FIG. 17. (a) The same as for Fig. 5 (b) for FCC lattice $\tau = 0.05$, at $T = 0.002t$, $U = 6.00t$. (b) The same as for Fig. 5 (a) for FCC lattice $\rho_{\text{FCC}}(\varepsilon)$ $\tau = 0.05$.

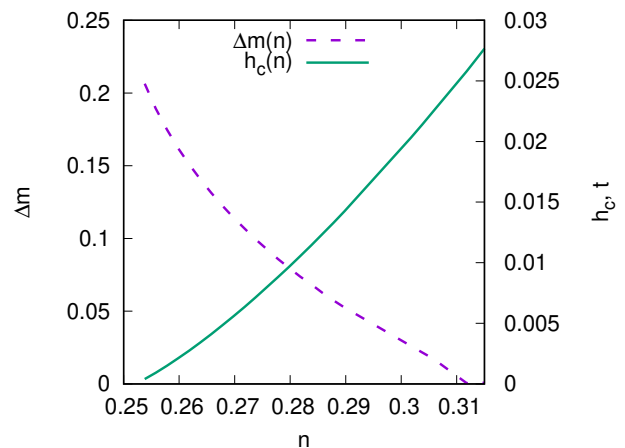


FIG. 18. The same as for Fig. 6 FCC lattice with $\tau = 0.05$, at $T = 0.002t$, $U = 6.00t$.

For such DOS, the magnetic field dependences at

the IEMM transition, see Fig. 17, exhibits remarkable paraprocess $h > h_c$, in contrast to the case $\tau = 0$ (see Fig. 14(a)).

The phase diagram $U-n$ (see Fig. 19) has a behavior, similar to that described earlier for $\tau = 0$ (see Fig. 16), but the filling interval, where IEMM transition occurs, is considerably reduced for all values of U .

However, the values of critical fields are strongly reduced too and become more physically reasonable, see Fig. 18.

In this case, saturated magnetism in critical fields is not observed in the whole IEMM transition region and appears only in FM region, being denoted as SFM region in Fig. 19.

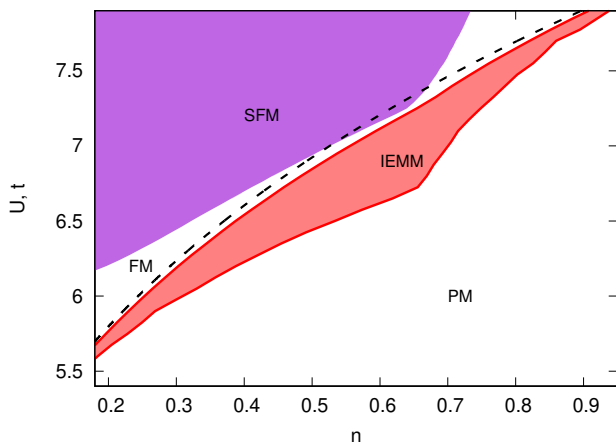


FIG. 19. Phase diagram in $U - n$ variables for FCC lattice at $\tau = 0.05$ and different temperatures: FM is ferromagnetic region, PM paramagnetic region. Within the latter, filled (IEMM) areas correspond to metamagnetism regions. The dotted line indicates the curve corresponding the Stoner criterion $U\rho(E_F) = 1$. The SFM region corresponds to the saturated ferromagnetism region.

3. $\tau \approx -1/2$

In this subsection the case of giant vHS at $\tau' \simeq -1/2$ for FCC lattice is considered, see Sec. II. At weak deviation of τ from $-1/2$, the giant VSH is transformed into a van Hove plateau. Two values close to $\tau = -1/2$ — $\tau = -0.52$ and -0.54 are chosen, see Fig. 4. In this case, the metamagnetic transition exists in a small filling interval, see Fig. 20. The critical magnetic fields have no anomalously large values, and for $\tau = -0.54$ h_c is an order of magnitude smaller than for DOS with $\tau = -0.52$ for the same parameters U and T . In such a situation, strong temperature dependences of critical field and magnetization jump are expected (see the corresponding experimental examples in the Introduction).

The region of the IEMM transition follows along the Stoner line, see Fig. 21. The filling interval where the transition is possible remains narrow for any values of U .

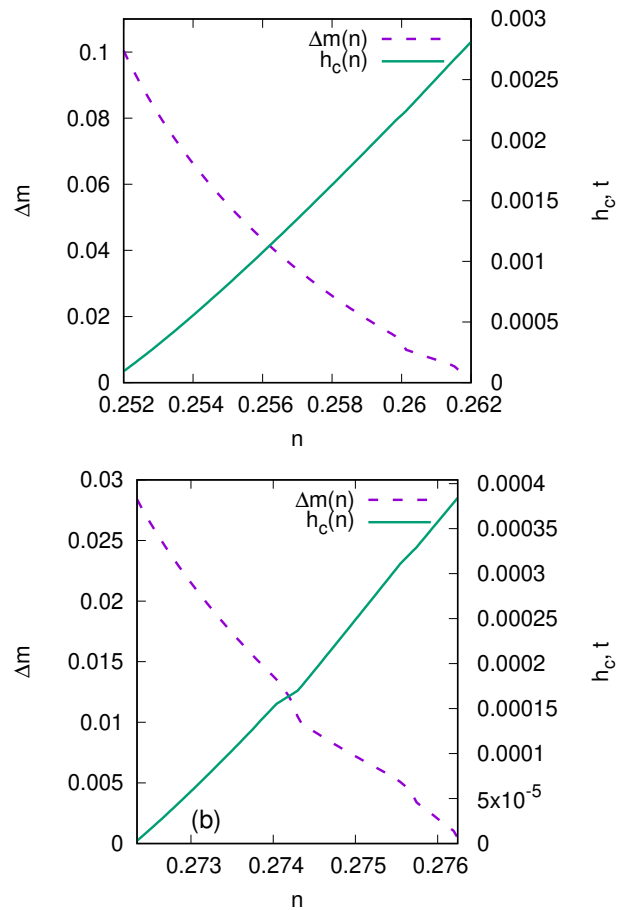


FIG. 20. The same as for Fig. 6 for FCC lattice $U = 1.50t$, $T = 2.00 \cdot 10^{-4}t$; (a) $\tau = -0.52$; (b) $\tau = -0.54$.

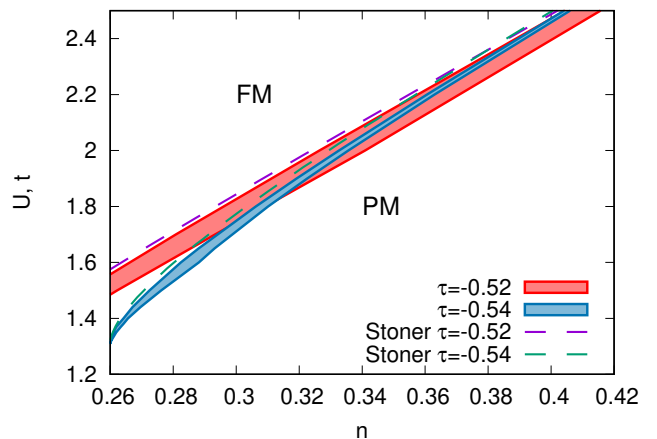


FIG. 21. Phase diagram for FCC lattice in $U - n$ variables at $T = 2.00 \cdot 10^{-4}t$. The filled regions denote IEMM regions at $\tau = -0.52$ and -0.54 , the dashed lines indicate the Stoner criterion (12), where E_F is taken for the paramagnetic phase for a given n .

IV. MAGNETIC PHASE TRANSITIONS: APPLICABILITY OF THE LANDAU THEORY

To explain the occurrence of IEMM transition, the Landau theory is typically used [38, 39]. In this Section we estimate the validity of the Landau theory for describing IEMM transitions in the Hubbard model. The Landau-theory expansion of the free energy has the form

$$F_{\text{Landau}}(T, n, h|m) = a_0(T, n) + a_2(T, n)m^2 + a_4(T, n)m^4 + a_6(T, n)m^6 - hm, \quad (24)$$

where explicit expression for coefficients a_i within HFA are written in the Appendix A. The stability of expansion (24) requires $a_6 > 0$. At given T, n, h , a state with m corresponding to global minimum of F_{Landau} with respect to m is established. In the case of second-order phase transition which occurs at $a_4 > 0$, negative (positive) a_2 values correspond to FM (PM) phase, and the transition between them ($a_2 = 0$) is continuous. Within HFA, the FM state condition $a_2 = (1/4)(\rho^{-1}(E_F) - U) < 0$ at $T = 0$ produces standard Stoner criterion, see Eq. (12). In the Stoner picture, small negative a_2 values correspond to weak itinerant ferromagnetism, whereas small positive a_2 to nearly ferromagnetic situation.

Negative a_4 can induce first-order magnetic phase transition at $a_2 > 0$. In this case, for the zero magnetic field ($h = 0$), when the condition $a_2 < a_c^{\text{II}}$ ($a_c^{\text{II}} = 3a_4^2/(5a_6)$) is satisfied the free energy has two local minima $m_1 = 0$ and $m_2 > 0$, and in the case $F_{\text{Landau}}(T, n, h = 0|m_1) < F_{\text{Landau}}(T, n, h = 0|m_2)$, a global minimum corresponds to the paramagnetic state. When the magnetic field h is turned on, both minimum levels are lowered proportionally to m_i and at a certain value h the minima will coincide $F_{\text{Landau}}(T, n, h|m_1) = F_{\text{Landau}}(T, n, h|m_2)$. At this value of magnetic field, the magnetization changes abruptly indicating the IEMM transition. For the chosen signs of the coefficients, ferromagnetic ordering requires fulfillment of the condition $a_2 < a_c^{\text{I}}$ ($a_c^{\text{I}} = a_4^2/(4a_6)$), which follows from $F_{\text{Landau}}(T, n, h = 0|m_1 = 0) > F_{\text{Landau}}(T, n, h = 0|m_2)$. In this case, negative value of a_4 ,

$$a_4 = \frac{1}{4} \frac{1}{16(\rho(E_F))^3} \left(\frac{(\rho'(E_F))^2}{\rho^2(E_F)} - \frac{\rho''(E_F)}{3\rho(E_F)} \right), T = 0,$$

considerably modifies the criterion of ferromagnetic ordering, thereby invalidating the Stoner criterion, see the phase diagrams. a_4 , being squared, should be sufficiently large, which can be achieved due to vHS at the PM phase Fermi level. On the basis of the corrected criterion of ferromagnetism ($a_2 < a_c^{\text{I}}$) and the condition for the existence of two local minima of the free energy ($a_2 < a_c^{\text{II}}$) we can write the condition for the IEMM transition

$$a_c^{\text{I}} < a_2 < a_c^{\text{II}}. \quad (25)$$

Since the Landau theory is constructed as an expansion in magnetization, it is not capable to describe the transition from saturated to non-saturated FM state.

Note that, generally speaking, higher-order expansion terms cannot be neglected, since they are physically related to the derivatives of bare DOS (see Appendix). Moreover, we will demonstrate that they can become large in the case of closeness of PM phase Fermi level to vHS.

Describing metamagnetism within the Landau expansion is possible only in the case of small magnetization, many works being devoted to this approach [4, 38, 39, 53–58]. Previously, the expansion of the free energy in powers of magnetization (Landau functional) was obtained in [38, 39]. In this section, we will compare the results of the Landau theory for the calculated coefficients $a_2(T, n)$, $a_4(T, n)$, $a_6(T, n)$ with the numerical solution of the equations (7–8), which will allow us to evaluate the limits of applicability of the Landau functional approach.

For example, we consider the case of a rectangular lattice with $\tau_a = 0.90$, $\tau = 0.20$, choosing the filling at which the IEMM transition occurs, $n = 0.62$, see Fig. 5. The temperature dependences of coefficients a_i are shown at Fig. 22(b). The coefficient $a_6(T, n) > 0$ at $T > 0.016t$ and $a_4(T, n) < 0$ at $T < 0.040t$. That is, the fulfillment of the condition for the $F_{\text{Landau}}(T, n|m)$ minimum is possible at $T > 0.016t$, but at $T > 0.040t$ the coefficient $a_4(T, n)$ becomes positive, and hence the second free energy minimum disappears, so that the IEMM transition is impossible. Comparison of F_{HFA} and F_{Landau} at zero magnetic field $h = 0$ and $U = 0$ in the temperature region $0.008 < T < 0.040t$ Fig. 22(a) shows good agreement for magnetization values down to $m = 0.05$. Thus, in this case, where the metamagnetic transition occurs in the region of magnetization $m < 0.05$, the results described by the Landau theory should agree well with those obtained from HFA. The m dependence of the free energy within HFA changes only weakly with temperature, see Fig. 22(a), whereas the free energy of the Landau theory has poor convergence to the value of $F_{\text{HFA}}(T, n|m)$ at $m > 0.06$, which becomes even worse with decreasing temperature. This feature strongly limits using the Landau expansion due to that a necessary number of expansion terms to be retained is *a priori* unknown.

The filling and temperature dependence of a_i is shown in Fig. 23. At filling values, which correspond to PM phase Fermi level coinciding with vHS, peaks also appear in the $a_i(n)$ dependence. An increase in temperature results in a decrease of peaks height. The coefficient $a_4(T, n)$ has a negative value at $0.55 < n < 0.63$ and $T = 0.016t$, which coincides with the region where IEMM transition occurs in mean-field calculations (see Fig. 7). For the applicability of Landau's theory, it is also necessary for the coefficient $a_6(T, n)$ to be positive (and substantially large) in the region where $a_4(T, n)$ is negative. As we can see from Fig. 23, $a_6(T, n)$ becomes positive only at temperatures greater than $T = 0.016t$ and in a very small filling region. Large a_i values indicate inapplicability of the expansion which is usually performed in the Landau theory.

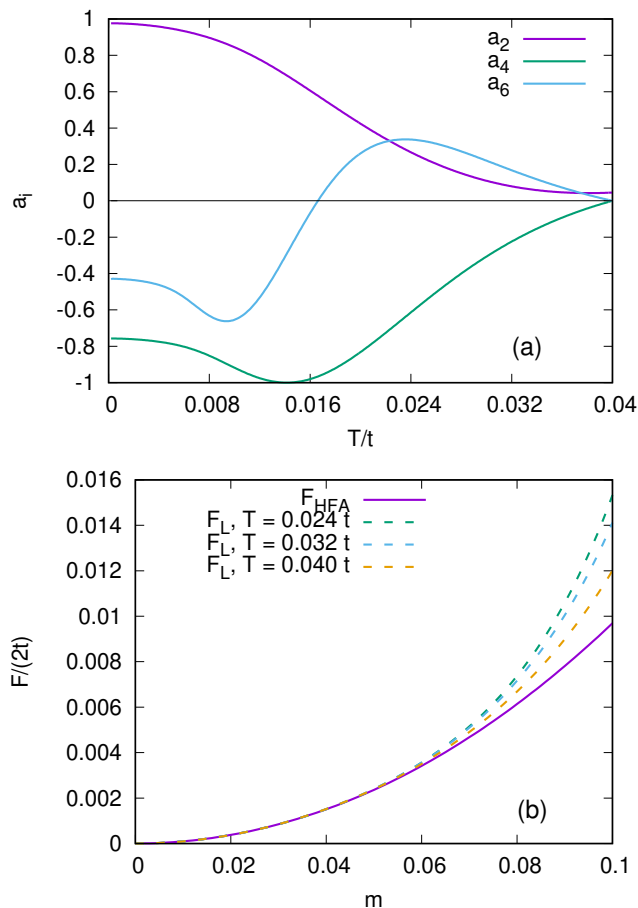


FIG. 22. (a) Dependence of the mean-field free energy $F_{\text{HFA}}(T, n|m)$ (solid lines) and Landau free energy $F_{\text{Landau}}(T, n|m)$ (dashed lines) on the magnetization m for different temperatures at $U = 0$ for rectangular lattice $\tau_a = 0.90$, $\tau = 0.20$ at $n = 0.62$. (b) Temperature dependence of the rescaled expansion coefficients $a_{2,4,6}(T, n)$.

By selecting the parameters corresponding to the conditions $a_2 > 0$, $a_4 < 0$, $a_6 > 0$: $U = 7.40t$, $T = 0.032t$, magnetic field dependences were constructed, Fig. 24. The results agree well up to $m = 0.02$. At these filling values, metamagnetism is already strongly suppressed by temperature. At $n = 0.57$, an IEMM transition occurs at magnetization value for which the results are already poorly consistent.

The Landau theory phase diagram is shown in Fig. 25. One can see that the possibility of the Landau theory to yield correct criterion of IEMM transition is restricted to the region of close vicinity of $a_4 = 0$ line. The extension of the validity region requires taking into account more and more terms of the Landau expansion. Thus the application of the Landau expansion to describe IEMM transition (25) (see Refs. 38 and 39) should be performed with a great caution.

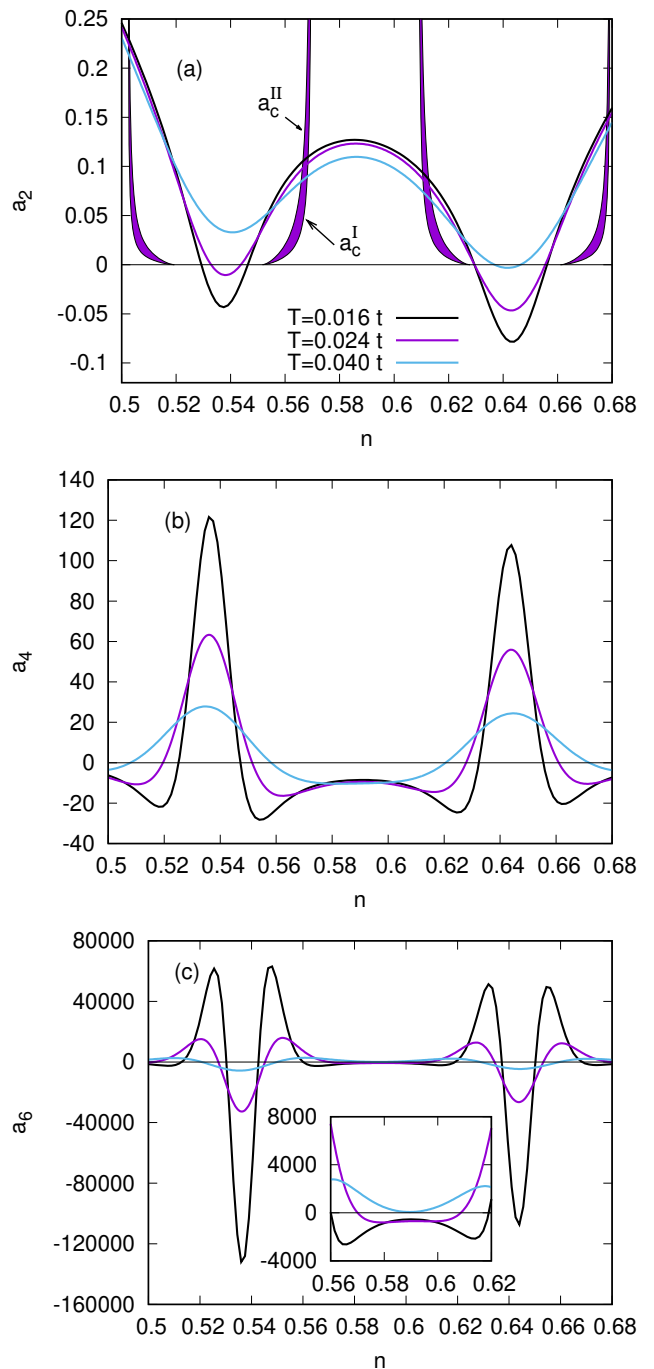


FIG. 23. Dependence on filling of the rescaled expansion coefficients a_i for different temperatures for rectangular lattice $\tau_a = 0.90$, $\tau = 0.20$ at $U = 7.00t$. (a) $a_2(n)$, filling indicates region $a_c^{\text{I}} < a_2 < a_c^{\text{II}}$ at $T = 0.024t$; (b) $a_4(n)$; (c) $a_6(n)$.

V. CONCLUSIONS

As discussed in the Introduction, itinerant metamagnetism occurs in the case of large positive DOS curvature. There are several factors which are favourable for this DOS form: splitting of vHS, reduced space dimensional-

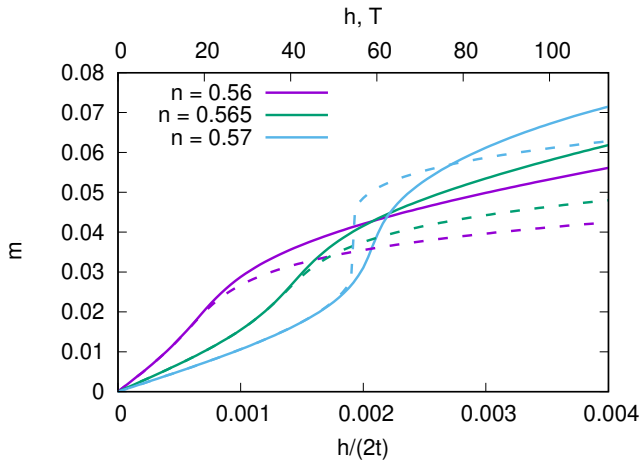


FIG. 24. Dependence of magnetization on magnetic field: comparison of numerical calculation with the Landau theory at different filling values $U = 7.40t$ for rectangular lattice $\tau_a = 0.90$, $\tau = 0.20$ at $T = 0.032t$. The solid line corresponds to calculations from the mean-field approximation, and the dashed line to those from the Landau theory.

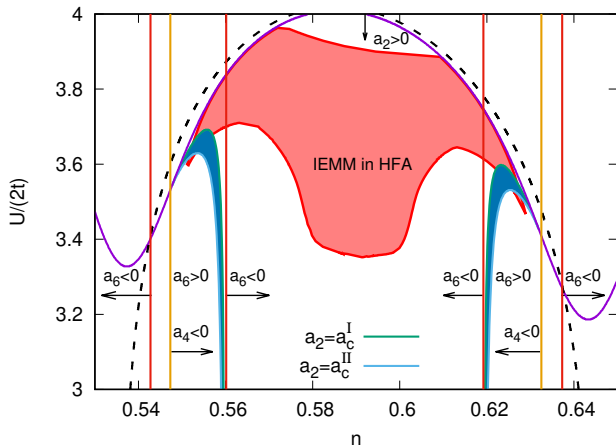


FIG. 25. Comparison of phase diagrams in $U - n$ variables obtained from the Landau theory and HFA for a rectangular lattice with $\tau_a = 0.9$, $\tau = 0.20$ at $T = 0.016t$. The blue area between the curves $a_2 = a_c^I$ and $a_2 = a_c^{II}$ corresponds to the region of IEMM transition according to the Landau theory.

ity (layered systems), hybridization in the case of degenerate electron bands. We have investigated the possibility of existence of metamagnetism for densities of states possessing peculiarities characteristic for these factors.

The splitting of vHS leads to the appearance of a region with strong positive curvature between vHS peaks, which may favorably affect the occurrence of metamagnetism in a large filling region. We have shown how such a splitting leads to a double-peak structure of the electronic DOS and the formation of a metamagnetic transition between ferromagnetic phases for a two-dimensional rectangular lattice. The metamagnetic transition is preserved by introducing hopping along the z -axis. At the

same time, the U -region where metamagnetism exists is narrowed owing to smoothing of two-dimensional lattice DOS peaks. However, a considerable metamagnetism region is found for an orthorhombic lattice.

An example of metamagnetism in systems with lowered dimensionality is provided by layered ruthenates $\text{Sr}_3\text{Ru}_2\text{O}_7$ and $\text{Sr}_4\text{Ru}_3\text{O}_{10}$ (see Introduction). As for three-dimensional systems, a scenario of metamagnetic transition induced by position of the Fermi level between two vHS peaks was suggested for metamagnetic transition in MnAs under pressure larger than 14.6 kbar [59].

For a FCC lattice with logarithmic divergence at the bottom of the band ($\tau = 0$), ferromagnetism has saturated nature, and the IEMM transition occurs in a wide filling region, but in anomalously strong magnetic fields. When considering the case $\tau = 0.05$, the logarithmic DOS divergence becomes smeared, and the critical magnetic fields of the IEMM transition become more realistic.

For the FCC lattice with $\tau \simeq -0.5$, metamagnetism arises at the position of the Fermi level near single vHS in the form of a plateau, in the region with a positive curvature. However, as reflected in the presented phase diagrams, the filling interval of existence of metamagnetism is not wide. Therefore we can conclude that the DOS structure is insufficient to observe the effect in a larger region for such a case. However, in this case we can expect low values of critical fields and strong temperature dependence of the magnetization jump. Further investigation of this dependence in the presence of vHS, as well as of non-trivial temperature dependence of magnetic susceptibility in the paramagnetic phase, would be of interest.

We have performed our consideration within the mean-field approximation. Unlike the finite-temperature case, this approach is, generally speaking, satisfactory at $T = 0$ (e.g., in the Moriya theory [47] the ground state is described by the Stoner theory, but spin fluctuations are important at finite T). However, in the presence of vHS the ground-state and low temperature renormalizations are expected to have strong parameter dependence. In particular, the treatment within functional renormalization group for 3D spectrum with giant vHS shows that in the absence of enhanced incommensurate magnetic fluctuation the Hubbard interaction U can be considered as a Coulomb interaction parameter being renormalized by scattering in particle-particle channel [44]. Thus we expect that correlation effects result in renormalization of the parameter U only. Other related cases are provided by the 2D situation with $t' \lesssim t'/2$ and systems with noticeable Fermi surface feature like nesting [60–63], where long-wave incommensurate fluctuations and corresponding scattering channel dominate.

Rather large critical U obtained for metamagnetic transition suggests that full-fledged theory of IEMM caused by vHS should concern both many-orbital effects and Hund's interaction compensating insufficiency of direct Coulomb interaction.

Our study of the applicability of Landau's theory for

metamagnetism has shown that an adequate description of this phenomenon is possible only when considering the terms in the expansion up to the eighth order and at high enough temperature, which strongly reduces the limits of applicability of Landau's theory to describe this phenomenon.

VI. ACKNOWLEDGMENTS

We are grateful to N. V. Mushnikov for fruitful discussions. The studies are partially supported by the state assignment of the Ministry of Science and Higher Education of the Russian Federation (theme "Quant" No. 122021000038-7) and by the Development Program of the Ural Federal University within the strategic academic leadership program "Priority-2030". Numerical computations were performed on the Uran supercomputer at the IMM UB RAS.

Appendix A: Landau expansion derivation

The coefficients a_2 , a_4 , a_6 in the free energy expansion (2) can be calculated from

$$a_2 = \frac{1}{4}(\Pi_0^{-1} - U), \quad (\text{A1})$$

$$a_4 = \frac{1}{4} \frac{1}{16\Pi_0^3} \left(\frac{\Pi_0'^2}{\Pi_0^2} - \frac{\Pi_0''}{3\Pi_0} \right), \quad (\text{A2})$$

$$a_6 = \frac{1}{4} \frac{1}{16} \frac{1}{24\Pi_0^5} \left(7 \left(\frac{\Pi_0'}{\Pi_0} \right)^4 - 7 \frac{\Pi_0'^2}{\Pi_0^3} \Pi_0'' + \frac{2}{3} \left(\frac{\Pi_0''}{\Pi_0} \right)^2 + \frac{\Pi_0' \Pi_0'''}{\Pi_0^2} - \frac{1}{15} \frac{\Pi_0''''}{\Pi_0} \right), \quad (\text{A3})$$

$$a_8 = \frac{1}{128\Pi_0^{13}} \left[17325\Pi_0\Pi_0'^4\Pi_0'' + 126\Pi_0^2\Pi_0'^2 \left(3\Pi_0\Pi_0'^4 - 50\Pi_0''^2 \right) - 28\Pi_0^3\Pi_0' \left(\Pi_0\Pi_0'^5 - 45\Pi_0^{(3)}\Pi_0'' \right) - 10395\Pi_0'^6 - 3150\Pi_0^2\Pi_0^{(3)}\Pi_0'^3 + \Pi_0^3 \left(280\Pi_0''^3 - 56\Pi_0\Pi_0'^4\Pi_0'' + \Pi_0 \left(\Pi_0\Pi_0^{(6)} - 35(\Pi_0^{(3)})^2 \right) \right) \right], \quad (\text{A4})$$

where zero wave vector polarization operator reads

$$\Pi_0 = \frac{1}{TN} \sum_{\mathbf{k}} \zeta \left(\frac{\epsilon_{\mathbf{k}} - E_F}{T} \right) \quad (\text{A5})$$

with $\zeta(x) = \frac{1}{4 \cosh^2 \frac{x}{2}}$, primes denote derivatives with respect to E_F argument.

-
- [1] E. Wohlfarth and P. Rhodes, Collective electron metamagnetism, *Philosophical Magazine* **7**, 1817 (1962).
 - [2] K. Adachi, M. Matsui, and M. Kawai, Further investigations on magnetic properties of $\text{Co}(\text{Se}_{1-x}\text{S}_x)_2$, ($0 \leq x \leq 1$), *Journal of the Physical Society of Japan* **46**, 1474 (1979).
 - [3] N. Mushnikov and T. Goto, Itinerant electron metamagnetism and magnetoelasticity of CoS_2 , *The Physics of Metals and Metallography* **93** (2002).
 - [4] T. Goto, Y. Shindo, H. Takahashi, and S. Ogawa, Magnetic properties of the itinerant metamagnetic system $\text{Co}(\text{S}_{1-x}\text{Se}_x)_2$ under high magnetic fields and high pressure, *Physical Review B* **56**, 14019 (1997).
 - [5] H. Yamada, Metamagnetic transition and susceptibility maximum in an itinerant-electron system, *Phys. Rev. B* **47**, 11211 (1993).
 - [6] H. Yamada and M. Shimizu, Metamagnetic transition of YCo_2 , *Journal of Physics F: Metal Physics* **15**, 175 (1985).
 - [7] T. Goto, K. Fukamichi, T. Sakakibara, and H. Komatsu, Itinerant electron metamagnetism in YCo_2 , *Solid state communications* **72**, 945 (1989).
 - [8] T. Goto, T. Sakakibara, K. Murata, H. Komatsu, and K. Fukamichi, Itinerant electron metamagnetism in YCo_2 and LuCo_2 , *Journal of magnetism and magnetic materials* **90**, 700 (1990).
 - [9] N. Mushnikov and T. Goto, Itinerant electron metamagnetism of $\text{Y}(\text{Co}_{1-x}\text{Al}_x)_2$ under high pressure and high magnetic fields, *Journal of Physics: Condensed Matter* **11**, 8095 (1999).
 - [10] T. Sakakibara, T. Goto, K. Yoshimura, M. Shiga, and Y. Nakamura, Itinerant electron metamagnetism in $\text{Y}(\text{Co}_{1-x}\text{Al}_x)_2$, *Physics Letters A* **117**, 243 (1986).
 - [11] V. Aleksandryan, A. Lagutin, R. Levitin, A. Markosyan, *et al.*, Metamagnetism of itinerant d-electrons in YCo_2 : Investigation of metamagnetic transitions in $\text{Y}(\text{Co}, \text{Al})_2$, *Sov. Phys.-JETP* **62** (1985).
 - [12] I. Gabelko, R. Levitin, A. Markosyan, and V. Snegirev, Onset of ferromagnetism in the band paramagnet LuCo_2 upon the replacement of cobalt by aluminum, *JETP Lett* **45** (1987).
 - [13] K. Fukamichi, T. Yokoyama, H. Saito, T. Goto, and H. Yamada, Magnetic phase diagrams of itinerant-electron metamagnetic $\text{Lu}(\text{Co}_{1-x}\text{M}_x)_2$ ($\text{M} = \text{Al}$ and Ga) laves-phase compounds, *Physical Review B* **64**, 134401 (2001).
 - [14] K. Yoshimura and Y. Nakamura, New weakly itinerant ferromagnetic system, $\text{Y}(\text{Co}_{1-x}\text{Al}_x)_2$, *Solid state communications* **56**, 767 (1985).
 - [15] D. S. Neznakhin, D. I. Radzivonchik, D. I. Gorbunov, A. V. Andreev, J. Šebek, A. V. Lukoyanov, and M. I. Bartashevich, Itinerant metamagnetic transition in the ferromagnet LuCo_3 induced by high field: Instability of the

- 3d-electron subsystem, Phys. Rev. B **101**, 224432 (2020).
- [16] D. Radzivonchik, D. Neznakhin, and A. Lukoyanov, Site-selective spin transition in LuCo_3 , Journal of Physics and Chemistry of Solids **163**, 110552 (2022).
- [17] R. S. Perry, L. M. Galvin, S. A. Grigera, L. Capogna, A. J. Schofield, A. P. Mackenzie, M. Chiao, S. R. Julian, S. I. Ikeda, S. Nakatsuji, Y. Maeno, and C. Pfleiderer, Metamagnetism and critical fluctuations in high quality single crystals of the bilayer ruthenate $\text{Sr}_3\text{Ru}_2\text{O}_7$, Phys. Rev. Lett. **86**, 2661 (2001).
- [18] G. Cao, L. Balicas, W. H. Song, Y. P. Sun, Y. Xin, V. A. Bondarenko, J. W. Brill, S. Parkin, and X. N. Lin, Competing ground states in triple-layered $\text{Sr}_4\text{Ru}_3\text{O}_{10}$: verging on itinerant ferromagnetism with critical fluctuations, Phys. Rev. B **68**, 174409 (2003).
- [19] N. Mushnikov, T. Goto, K. Kamishima, H. Yamada, A. Andreev, Y. Shiokawa, A. Iwao, and V. Sechovsky, Magnetic properties of the 5f itinerant electron magnet UCoAl under high pressure, Physical Review B **59**, 6877 (1999).
- [20] N. Mushnikov, T. Goto, A. Andreev, V. Sechovský, and H. Yamada, Effect of external pressure on the magnetism of $\text{UCo}_{0.98}\text{Fe}_{0.02}\text{Al}$, Physical Review B **66**, 064433 (2002).
- [21] H. Yamada, K. Fukamichi, and T. Goto, Itinerant-electron metamagnetism and strong pressure dependence of the curie temperature, Physical Review B **65**, 024413 (2001).
- [22] D. Aoki, K. Ishida, and J. Flouquet, Review of u-based ferromagnetic superconductors: comparison between UGe_2 , URhGe , and UCoGe , Journal of the Physical Society of Japan **88**, 022001 (2019).
- [23] D. Aoki, A. Huxley, E. Ressouche, D. Braithwaite, J. Flouquet, J.-P. Brison, E. Lhotel, and C. Paulsen, Coexistence of superconductivity and ferromagnetism in URhGe , Nature **413**, 613 (2001).
- [24] N. Huy, A. Gasparini, D. De Nijs, Y. Huang, J. Klaasse, T. Gortenmulder, A. de Visser, A. Hamann, T. Görlach, and H. v. Löhneysen, Superconductivity on the border of weak itinerant ferromagnetism in UCoGe , Physical review letters **99**, 067006 (2007).
- [25] M. Szlowska, M. Majewicz, D. A. Kowalska, and D. Kaczorowski, Metamagnetic transition in single-crystalline UIr_2Si_2 , Scientific Reports **13**, 14772 (2023).
- [26] A. McCollam, M. Fu, and S. R. Julian, Lifshitz transition underlying the metamagnetic transition of UPt_3 , Journal of Physics: Condensed Matter **33**, 075804 (2020).
- [27] A. Fujita, Y. Akamatsu, and K. Fukamichi, Itinerant electron metamagnetic transition in $\text{La}(\text{Fe}_x\text{Si}_{1-x})_{13}$ intermetallic compounds, Journal of Applied Physics **85**, 4756 (1999).
- [28] A. Fujita and K. Fukamichi, Giant volume magnetostriction due to the itinerant electron metamagnetic transition in $\text{La}(\text{FeSi})_{13}$ compounds, IEEE transactions on magnetics **35**, 3796 (1999).
- [29] A. Fujita, K. Fukamichi, J.-T. Wang, and Y. Kawazoe, Large magnetovolume effects and band structure of itinerant-electron metamagnetic $\text{La}(\text{Fe}_x\text{Si}_{1-x})_{13}$ compounds, Physical Review B **68**, 104431 (2003).
- [30] S. Gama, A. A. Coelho, A. de Campos, A. M. G. Carvalho, F. C. Gandra, P. J. von Ranke, and N. A. de Oliveira, Pressure-induced colossal magnetocaloric effect in MnAs , Physical review letters **93**, 237202 (2004).
- [31] O. Tegus, E. Brück, L. Zhang, K. Buschow, F. De Boer, *et al.*, Magnetic-phase transitions and magnetocaloric effects, Physica B: Condensed Matter **319**, 174 (2002).
- [32] V. K. Pecharsky and K. A. Gschneidner, Jr., Giant magnetocaloric effect in $\text{Gd}_5(\text{Si}_2\text{Ge}_2)$, Phys. Rev. Lett. **78**, 4494 (1997).
- [33] V. Taufour, D. Aoki, G. Knebel, and J. Flouquet, Tricritical point and wing structure in the itinerant ferromagnet UGe_2 , Physical review letters **105**, 217201 (2010).
- [34] S. Saxena, P. Agarwal, K. Ahilan, F. Grosche, R. Haselwimmer, M. Steiner, E. Pugh, I. Walker, S. Julian, P. Monthoux, *et al.*, Superconductivity on the border of itinerant-electron ferromagnetism in UGe_2 , Nature **406**, 587 (2000).
- [35] N. Kimura, M. Endo, T. Isshiki, S. Minagawa, A. Ochiai, H. Aoki, T. Terashima, S. Uji, T. Matsumoto, and G. Lonzarich, de haas-van alphen effect in ZrZn_2 under pressure: crossover between two magnetic states, Physical review letters **92**, 197002 (2004).
- [36] M. Uhlarz, C. Pfleiderer, and S. Hayden, Quantum phase transitions in the itinerant ferromagnet ZrZn_2 , Physical review letters **93**, 256404 (2004).
- [37] K. Sandeman, G. Lonzarich, and A. Schofield, Ferromagnetic superconductivity driven by changing fermi surface topology, Physical review letters **90**, 167005 (2003).
- [38] M. Shimizu, Itinerant electron metamagnetism, Journal de Physique **43**, 155 (1982).
- [39] R. Levitin and A. S. Markosyan, Itinerant metamagnetism, Soviet Physics Uspekhi **31**, 730 (1988).
- [40] P. A. Igoshev and V. Y. Irkhin, Giant density-of-states van hove singularities in the face-centered cubic lattice, Physics Letters A **438**, 128107 (2022).
- [41] M. M. Wysokiński, M. Abram, and J. Spałek, Criticalities in the itinerant ferromagnet UGe_2 , Physical Review B **91**, 081108 (2015).
- [42] A. Berridge, Role of band structure in the thermodynamic properties of itinerant metamagnets, Physical Review B **83**, 235127 (2011).
- [43] H. Yamase, Ferromagnetic and metamagnetic transitions in itinerant electron systems: a microscopic study, New Journal of Physics **25**, 033004 (2023).
- [44] P. A. Igoshev and A. A. Katanin, Ferromagnetic instability in itinerant fcc lattice electron systems with higher-order van hove singularities: Functional renormalization group study, Physical Review B **107**, 115105 (2023).
- [45] P. A. Igoshev and I. A. Nekrasov, Inverse magnetocaloric effect and phase separation induced by giant van hove singularity in itinerant ferromagnetic metal, Phys. Rev. B **110**, 134406 (2024).
- [46] M. Ulmke, Ferromagnetism in the hubbard model on fcc-type lattices, The European Physical Journal B - Condensed Matter and Complex Systems **1**, 301 (1998).
- [47] T. Moriya, Spin fluctuations in itinerant electron magnetism (1985).
- [48] P. A. Igoshev, E. E. Kokorina, and I. A. Nekrasov, Investigation of the magnetocaloric effect in correlated metallic systems with van hove singularities in the electron spectrum, Physics of Metals and Metallography **118**, 207–216 (2017).
- [49] P. A. Igoshev and V. Y. Irkhin, Giant van hove density of states singularities and anomalies of electron and magnetic properties in cubic lattices, Physics of Metals and Metallography **120**, 1282 (2019).

- [50] P. A. Igoshev and V. Y. Irkhin, Electron spectrum topology and giant singularities of the electron density of states in cubic lattices, *JETP Letters* **110**, 727 (2019).
- [51] R. J. Jelitto, The density of states of some simple excitations in solids, *Journal of Physics and Chemistry of Solids* **30**, 609 (1969).
- [52] M. Ulmke, Ferromagnetism in the hubbard model on fcc-type lattices, *The European Physical Journal B-Condensed Matter and Complex Systems* **1**, 301 (1998).
- [53] H. Yamada, Metamagnetic transition and susceptibility maximum in an itinerant-electron system, *Physical Review B* **47**, 11211 (1993).
- [54] T. Goto, K. Fukamichi, and H. Yamada, Itinerant electron metamagnetism and peculiar magnetic properties observed in $3d$ and $5f$ intermetallics, *Physica B: Condensed Matter* **300**, 167 (2001).
- [55] H. Yamada and T. Goto, Itinerant-electron metamagnetism and giant magnetocaloric effect, *Physical Review B* **68**, 184417 (2003).
- [56] D. Belitz, T. Kirkpatrick, and J. Rollbühler, Tricritical behavior in itinerant quantum ferromagnets, *Physical review letters* **94**, 247205 (2005).
- [57] H. Yamada, $P - T - B$ magnetic phase diagram of itinerant-electron metamagnets, *Physica B: Condensed Matter* **391**, 42 (2007).
- [58] A. Berridge, S. Grigera, B. Simons, and A. Green, Magnetic analog of the Fulde-Ferrell-Larkin-Ovchinnikov phase in $\text{Sr}_3\text{Ru}_2\text{O}_7$, *Physical Review B* **81**, 054429 (2010).
- [59] H. Yamada and K. Terao, Itinerant-electron metamagnetism of MnSi at high pressure, *Phys. Rev. B* **59**, 9342 (1999).
- [60] A. A. Katanin and A. P. Kampf, Renormalization group analysis of magnetic and superconducting instabilities near van hove band fillings, *Phys. Rev. B* **68**, 195101 (2003).
- [61] P. A. Igoshev, A. A. Katanin, and V. Y. Irkhin, Magnetic fluctuations and itinerant ferromagnetism in two-dimensional systems with van Hove singularities, *Journal of Experimental and Theoretical Physics* **105**, 1043 (2007).
- [62] P. A. Igoshev, V. Y. Irkhin, and A. A. Katanin, Magnetic fluctuations and self-energy effects in two-dimensional itinerant systems with a van hove singularity in the electronic spectrum, *Phys. Rev. B* **83**, 245118 (2011).
- [63] A. A. Stepanenko, D. O. Volkova, P. A. Igoshev, and A. A. Katanin, Kohn anomalies in momentum dependence of magnetic susceptibility of some three-dimensional systems, *Journal of Experimental and Theoretical Physics* **125**, 879 (2017).